


The Influence of Positioning of the Nellix Endovascular Aneurysm Sealing System on Suprarenal and Renal Flow: An In Vitro Study

Journal of Endovascular Therapy
 2017, Vol. 24(5) 677–687
 © The Author(s) 2017
 Reprints and permissions:
sagepub.com/journalsPermissions.nav
 DOI: 10.1177/1526602817719465
www.jevt.org


Johannes T. Boersen, MSc^{1,2}, Erik Groot Jebbink, MSc^{1,3},
 Lennart Van de Velde, BSc¹, Michel Versluis, PhD^{3,4},
 Guillaume Lajoinie, PhD³, Cornelius H. Slump, PhD⁴,
 Jean-Paul P. M. de Vries, MD, PhD², and Michel M. P. J. Reijnen, MD, PhD¹

Abstract

Purpose: To examine the influence of device positioning and infrarenal neck diameter on flow patterns in the Nellix endovascular aneurysm sealing (EVAS) system. **Methods:** The transition of the aortic flow lumen into two 10-mm-diameter stents after EVAS creates a mismatched area. Flow recirculation may affect local wall shear stress (WSS) profiles and residence time associated with atherosclerosis and thrombosis. To examine these issues, 7 abdominal aortic aneurysm flow phantoms were created, including 3 unstented controls and 3 stented models with infrarenal neck diameters of 24, 28, and 32 mm. Stents were positioned within the instructions for use (IFU). Another 28-mm model was created to evaluate lower positioning of the stents outside the IFU (28-mm LP). Flow was visualized using optical particle imaging velocimetry (PIV) and quantified by time-averaged WSS (TAWSS), oscillatory shear index (OSI), and relative residence time (RRT) in the aorta at the anteroposterior (AP) midplane, lateral midplane, and renal artery AP midplane levels. **Results:** Flow in the aorta AP midplane was similar in all models. Vortices were observed in the stented models in the lateral midplane near the anterior and posterior walls. In the 32-mm IFU and 28-mm LP models, a steady state of vortices appeared, with varying location during a cycle. In all models, a low TAWSS ($<10^{-2}$ Pa) was observed at the anterior wall of the aorta with peak OSI of 0.5 and peak RRT of 10^4 Pa⁻¹. This region was more proximally located in the stented models. The 24- and 28-mm IFU models showed flow with a higher velocity at the renal artery inflow compared to controls. TAWSS in the renal artery was lower near the orifice in all models, with the largest area in the 24-mm IFU model. OSI and RRT in the renal artery were near zero for all models. **Conclusion:** EVAS enhances vorticity proximal to the seal zone, especially with lower positioning of the device and in larger neck diameters. Endobags just below the renal artery affect the flow profile in a minor area of this artery in 24- and 28-mm necks, while lower stent positioning does not influence the renal artery flow profile.

Keywords

abdominal aortic aneurysm, aneurysm neck, atherosclerosis, endovascular aneurysm sealing, flow model, hemodynamics, neck diameter, renal artery, stent design, vorticity, wall stress

Introduction

Endovascular aneurysm sealing (EVAS) with the Nellix endosystem (Endologix Inc, Irvine, CA, USA) enables treatment of abdominal aortic aneurysms (AAA) based on in situ polymer filling of endobags that surround dual covered cobalt-chromium stents.^{1,2} The two 10-mm-diameter stents provide flow lumens to both limbs. The intended position of the endosystems according to the instructions for use (IFU) is with the proximal edge of the endobags just below the distal edge of the most caudal renal artery (RA).

¹Department of Surgery, Rijnstate Hospital, Arnhem, the Netherlands

²Department of Vascular Surgery, St Antonius Hospital, Nieuwegein, the Netherlands

³Department of Physics of Fluids, Faculty of Science and Technology, Technical University of Twente, Enschede, the Netherlands

⁴MIRA Institute for Biomedical Technology and Technical Medicine, University of Twente, Enschede, the Netherlands

Corresponding Author:

Johannes T. Boersen, MSc, Department of Vascular Surgery, St Antonius Hospital, Koekoekslaan 1, 3430 EM Nieuwegein, the Netherlands.

Email: j.boersen@antoniuziekenhuis.nl

The stents should therefore be positioned not higher than 4 mm (the portion of uncovered stent above the endobag) across the RA orifice to prevent (partial) coverage of the RA orifice by endobag material. The endosystem was designed to reduce reinterventions, mainly for type II endoleaks, which are relatively common following endovascular aneurysm repair (EVAR) with standard modular grafts. The clinical relevance of type II endoleak remains unclear and is the subject of ongoing debate. Generally, treatment is not performed if aneurysm growth is <10 mm during follow-up,³ but this threshold had not been validated. Low incidences of endoleaks and reinterventions have been reported with EVAS after 1 year, including clinical application of the device according to and outside the IFU.^{4,5}

The transition of the aortic flow lumen into the 2 stents induces a mismatched area between the aortic flow lumen and these stents, and a cul-de-sac⁶ may form between the RA and the upper margin of the endobags when the stents are positioned low in the neck. The design with 10-mm-diameter stents results in an uneven area reduction, especially in a larger diameter aorta. This mismatched area may result in recirculation of flow with vortex formation and stasis or stagnant flow that has been associated with thrombus formation.^{7,8} Wall shear stress (WSS) is defined as the force acting parallel to the vessel wall and is related to the flow profile. Baseline WSS in arteries has been reported in a range of 1 to 7 Pa *in vivo*.^{8,9} A very low average WSS, that is, 10^{-2} Pa, has been associated with enhanced atherosclerosis and blood coagulation^{8,10} and may be observed in areas with recirculating flow. Moreover, strong oscillations in WSS (ie, changes in flow and WSS direction) have been associated with enhanced atherosclerotic lesion formation.^{11,12}

In this *in vitro* study, the impact of the Nellix endosystem position on flow proximal to the seal zone and in the RA was evaluated, while also comparing different infrarenal neck diameters.

Methods

Flow Phantoms

Seven transparent silicone (Sylgard 184; Dow Corning GmBH, Wiesbaden, Germany) flow phantoms of an infrarenal AAA were created (Figure 1). Transparency was required for optical access for laser particle imaging velocimetry (PIV). The infrarenal neck length was set at 15 mm and the maximum AAA diameter was 55 mm. Anteroposterior (AP) aortoiliac angulations were excluded to facilitate 2-dimensional (2D) imaging of the flow at the lumen midplane. The infrarenal aortic neck diameter varied between the models to study the influence of the infrarenal neck diameter on flow proximal to the endobags. AAA models with infrarenal neck diameters of 24, 28, and 32 mm were created, including 1

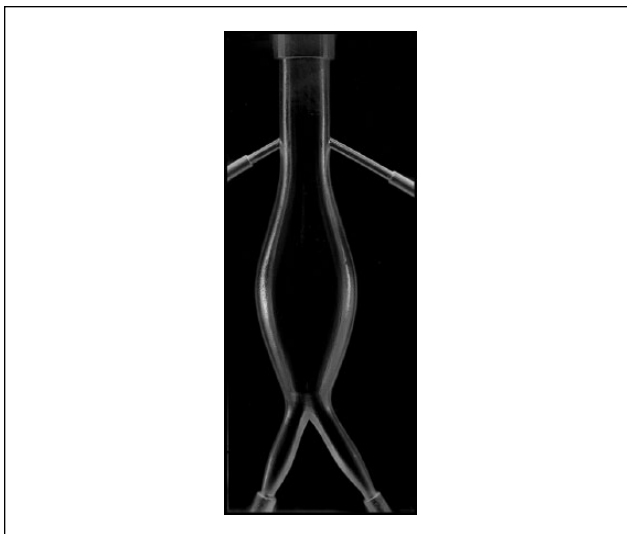


Figure 1. Flow phantom of abdominal aortic aneurysm.

unstented control and 1 stented model of each specific model. The stents were positioned according to the IFU, and these are referred to as the IFU models in this study. Another model with an infrarenal neck diameter of 28 mm was created to study the influence of an intentionally lower positioning (LP) of the endosystem, which is outside the IFU, and is referred to as the 28-mm LP model in this study.

Two Nellix endosystems with a length of 150 mm (NX 10-150) were implanted with an intended fill pressure of 180 mm Hg. The proximal edge of the endobag was positioned at the distal margin of the most caudal RA (Figure 2A, B, and D). In the 28-mm LP model the top of the stent was positioned at the distal margin of the most caudal RA, ~4 mm lower than the other configurations (Figure 2C). The implantation of the covered stents was performed by 2 physicians experienced with the EVAS endosystem (J.V., M.R.). After Nellix deployment the models were flushed with warm water (~37°C) to mimic *in vivo* conditions required for polymer curing. The phantoms were stored in a 0.9% saline solution and isolated from direct light sources to optimize conditions for polymer preservation for 2 to 3 weeks until the flow studies were completed.

Flow Characteristics

The flow setup was based on a 2-element windkessel.¹³ Both renal and iliac branches had dedicated peripheral resistance settings to adjust the outflow. The windkessel conditions were applied only to the iliac outflow, as the kidneys are a low-compliance part of the system showing very limited backflow *in vivo*. The compliance of both iliac arteries was combined into 1 compliance and 1 peripheral resistance. The difference in resistance between the renal arteries and iliac arteries was established by a larger

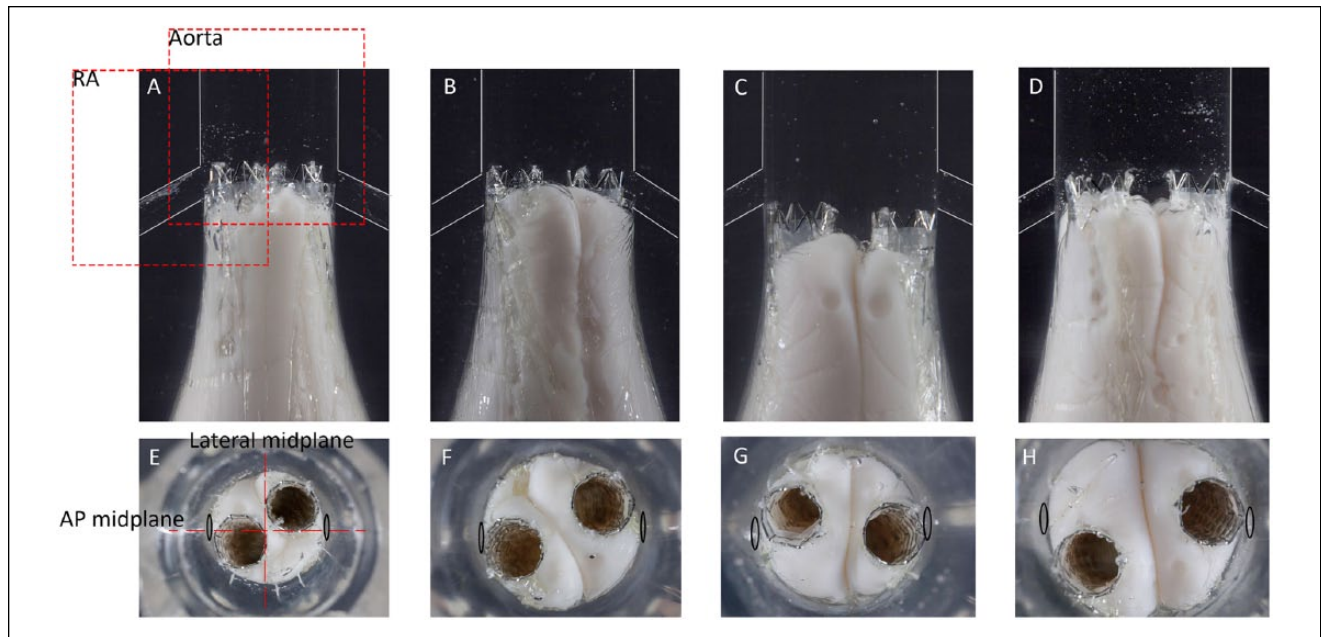


Figure 2. Frontal (A-D) and top views (E-H) of the stented models: (A, E) 24-mm IFU, (B, F) 28-mm IFU, (C, G) 28-mm low positioning, and (D, H) 32-mm IFU. The regions of interest are indicated in A and orientation of the planes in E. The renal orifice is indicated in the top view by a black circle that is drawn around the orifice. IFU, instructions for use.

diameter of the iliac artery (8 mm) in comparison with the renal artery (6 mm) at a comparable flow per branch (400 mL/min). The flow tests were performed under physiological resting conditions with a heart rate of 60 beats per minute, a blood pressure of 120/80 mm Hg, and a peripheral compliance of 1.1 mL/mm Hg. The inflow waveform was based on previous reported in vivo duplex ultrasound measurements with an average flow rate of 1.6 L/min (peak flow 3.6 L/min).¹⁴ A blood-mimicking fluid (BMF) was used with a dynamic viscosity comparable to blood (dynamic viscosity of 4.3 cP; density of 1.2 g/mL).¹⁵ The flow passed through a 1.2-m tube before it entered into the model, ensuring a fully developed laminar flow at the model inlet.

Flow Visualization

The flow was visualized with laser particle imaging velocimetry (PIV), based on imaging of fluorescent particles that accurately follow the fluid stream. Fluorescent polymethylmethacrylate particles measuring 1 to 20 μm in size with a density of 1190 kg/m³ (Rhodamine; Dantec Dynamics A/S, Skovlunde, Denmark) were dissolved in water, and the solution was mixed with the BMF. A 532-nm continuous wave laser (5W DPSS laser; Cohlibri, Lightline, Osnabruck, Germany) was used to illuminate a 2D layer of fluid (<1 mm) in the midplane of the flow lumen. The flow was captured in 3 planes: the AP midplane upstream of the proximal seal zone, the lateral midplane upstream of the proximal

seal zone, and the AP midplane of the right RA. To visualize the lateral plane, the model was turned by 90°. The regions of interest and orientation of the planes are indicated in Figure 2A and E, respectively. Full frame (1024×1024 pixels) images were captured with a high-speed camera (FASTCAM SAX-2; Photron Inc, West Wycombe, UK) at a rate of 1000 frames per second for a period of 10 seconds. The imaging plane dimension was ~5×5 cm, which resulted in a spatial resolution of 0.04 mm.

In-house scripts built for Matlab (R2016a; Mathworks, Natick, MA, USA) were used for automated wall detection to segment the flow lumen with fluorescent particles in the PIV images. PIVlab (open source toolbox, Matlab)¹⁶ was used to calculate the average displacement of particles in the fluid by calculating cross-correlations between subsequent frames. Velocity vectors were averaged over 10 cardiac cycles and displayed in Tecplot (360 EX 2016 R1; Tecplot, Bellevue, WA, USA). In addition, the average vorticity (s^{-1}) over a cardiac cycle was calculated to display regions of flow recirculation. The magnitude represents the amount of recirculation in a region, and the positive and negative signs represent the direction of the flow counterclockwise and clockwise, respectively.

WSS Calculations

Flow was quantified by time-averaged WSS (TAWSS; Pa), the oscillatory shear index (OSI; dimensionless),¹⁷ and the

relative residence time (RRT; Pa⁻¹).¹⁸ These parameters were calculated for the lateral and anterior aortic wall, which were both on the laser entry side for the different 2D imaging planes (AP and lateral) and therefore had the most reliable signal.

WSS was calculated by multiplying the viscosity of the BMF with the shear rate, defined by the velocity gradient parallel to the vessel wall (Equation 1). The calculations of the velocity gradient near the vessel wall included the flow velocity profile over 50% of the flow lumen length and a forced zero velocity at the vessel wall. TAWSS was calculated by averaging the WSS in a single point at the wall over 1 cardiac cycle.

The OSI (Equation 2) is defined by the ratio of positive and negative WSS areas under the WSS vs time curve during 1 cardiac cycle and is therefore a measure for the oscillatory behavior of the flow. OSI is 0 when WSS is unidirectional during the cardiac cycle. The maximum OSI is 0.5, indicating equal positive and negative WSS areas under the WSS vs time curve, referred to as high oscillatory shear. OSI can indicate areas of flow reversal; however, WSS magnitude is not taken into account. Strong oscillatory flows can exhibit the same OSI as very slow flows with the same waveform.

The RRT was introduced to incorporate the level of WSS and its oscillatory behavior.¹⁸ The RRT is a measure for residence time of particles near the vessel wall. With the given equation (Equation 3) OSI modifies the effect of the WSS on the RRT and near wall interactions. Relatively high values present potential regions with flow recirculation compared to regions with a RRT near zero.

WSS, OSI, and RRT were plotted vs the axial distance along the vessel wall to identify regions with unfavorable flow conditions associated with an enhanced atherosclerosis and thrombosis, that is, low TAWSS, peak OSI (0.5), and peak RRT.

$$\frac{1}{T} \int_0^T |\tau_w| dt \quad (1)$$

$$\frac{1}{2} \left(1 - \frac{\left| \int_0^T \tau_w dt \right|}{\int_0^T |\tau_w| dt} \right) \quad (2)$$

$$\frac{1}{(1 - 2 \cdot \text{OSI}) \cdot |\text{TAWSS}|} \quad (3)$$

Results

Suprarenal Aorta

The peak systolic velocity in the central lumen of the suprarenal aorta was comparable for the controls and

respective IFU models. The (peak) velocity was lower in models with a larger aortic diameter compared with a smaller diameter (around 16 cm/s, 14 cm/s, and 12 cm/s, respectively, for the 24-, 28-, and 32-mm models and respective IFU models). The flow profile in the AP midplane was comparable between the controls and IFU models; flow from the infrarenal aorta or stents recirculated into the RAs during the end-systolic phase, and retrograde flow was observed near the lateral suprarenal aortic wall (Videos 1, 2, and 3, available online). Also, the flow profile in the AP midplane of the 28-mm LP model was comparable to control (Video 4).

The controls and IFU models showed a different flow profile in the lateral midplane. The controls demonstrated retrograde flow near the anterior and posterior aortic wall (juxtarenal and suprarenal) during the end-systolic phase. In the IFU models, retrograde flow was also present, but additional vortex formation was observed proximal to the endobags near the anterior and posterior walls. In the 24- and 28-mm IFU models the vortex intensity decayed at the end of a cardiac cycle (Videos 5 and 6), whereas in the 32-mm IFU model (Video 7) the vortices appeared to have a steady state, although changing location during the cycle. The average vorticity over a cardiac cycle is displayed in Figure 3. The vorticity proximal to the endobags was larger in the 32-mm IFU model compared to the 24- and 28-mm IFU models and controls. In addition, the vorticity proximal to the endobags was larger in the 28-mm LP model (Figure 4), in which a steady appearance of vortices was also observed near the anterior and posterior walls. This was not the case in the 28-mm control and 28-mm IFU models (Videos 6 and 8).

TAWSS in the suprarenal aorta varied in a range from 0 to 1.2 Pa; both the controls and IFU models showed areas of low TAWSS at the anterior wall. In the control, this region was juxtarenal, while in the IFU models, the location was transferred proximally (-0.4 to -0.8 cm) and proximal to the endobags in regions of enhanced vorticity (Figure 5). In the 28-mm LP model, the location of low TAWSS was also more cranial compared to the control at -0.4 cm distance from the RA orifice (Figure 6). The OSI and RRT in the aorta were in a comparable range for the controls and stented models. The OSI in the aorta varied from 0 to 0.5, and the RRT varied from 0 to 10⁴ Pa⁻¹. The locations of peak OSI and peak RRT in the suprarenal aorta were in the same location as the regions that showed the lowest TAWSS. The axial distance of the regions was in the order of millimeters and was the largest in the 32-mm IFU model (0.2–0.3 cm).

Renal Artery

The 24- and 28-mm IFU models showed a stronger jet flow at the RA orifice with a higher peak velocity compared to

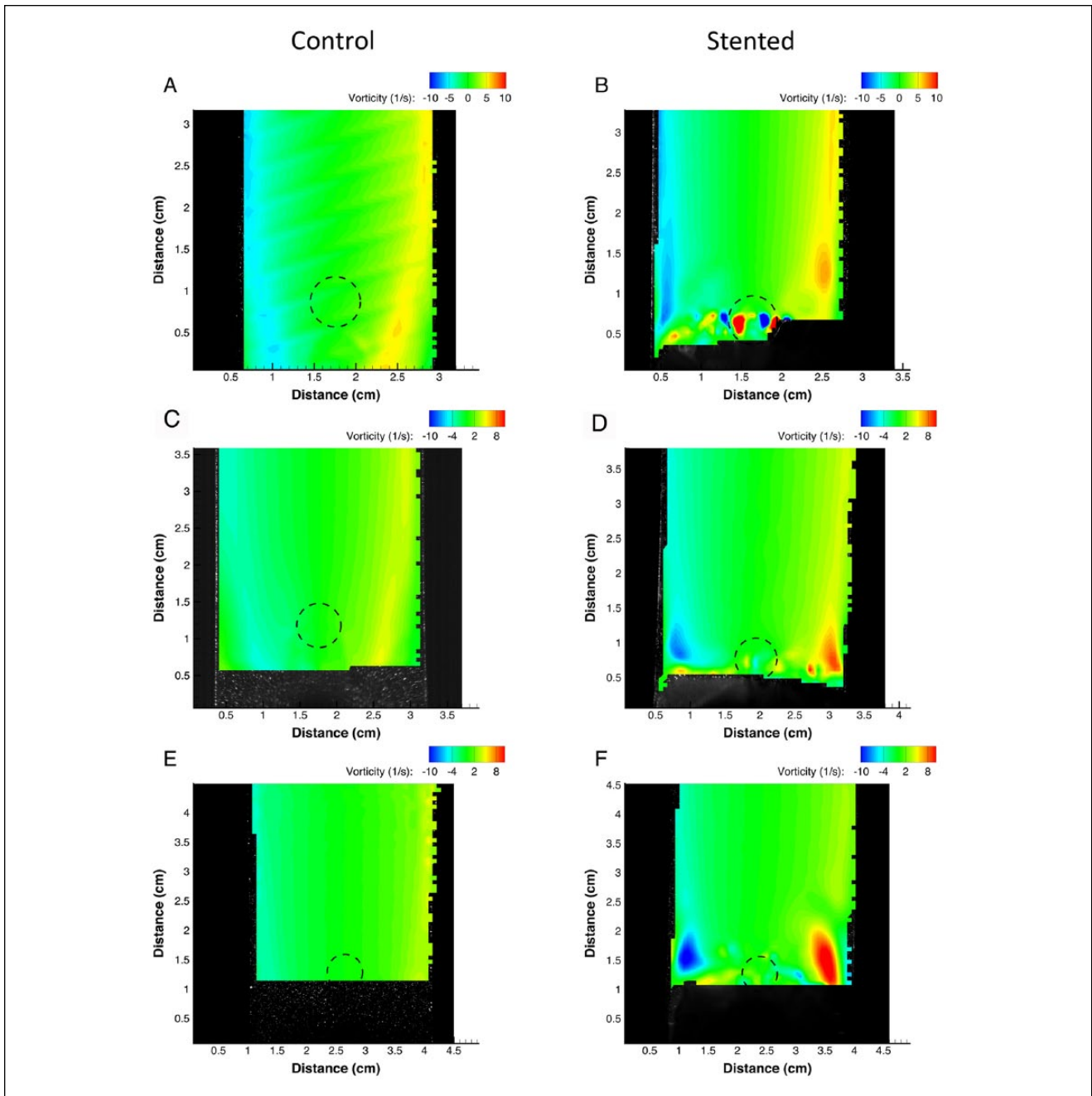


Figure 3. The average vorticity near the anterior and posterior wall in the (left) lateral midplane. The left figures show the unstented controls and right figures the respective models with Nellix endosystem implanted: (A) 24-mm control, (B) 24-mm IFU model, (C) 28-mm control, (D) 28-mm IFU model, (E) 32-mm control, (F) 32-mm IFU model. The black dashed circle indicates the renal artery orifice. IFU, instructions for use.

controls (Figure 7; Video 9). The maximum velocity in the RA was 85 cm/s in the 28-mm IFU model compared to 50 cm/s in the respective control. The 32-mm IFU model and 28-mm LP model showed a comparable flow profile and velocity in the RA flow compared to controls (Figure 7E and F and Figure 8A and C).

TAWSS in the RA was in a range of 0 to 2.3 Pa, with regions of lower TAWSS near the RA orifice in all models including controls (Figure 9). This region was largest on the caudal wall in the 24-mm IFU model with 0.5 to 1 Pa over a distance of 2 mm from the RA orifice (Figure 9B). The 28-mm LP model showed no areas of lower TAWSS in the

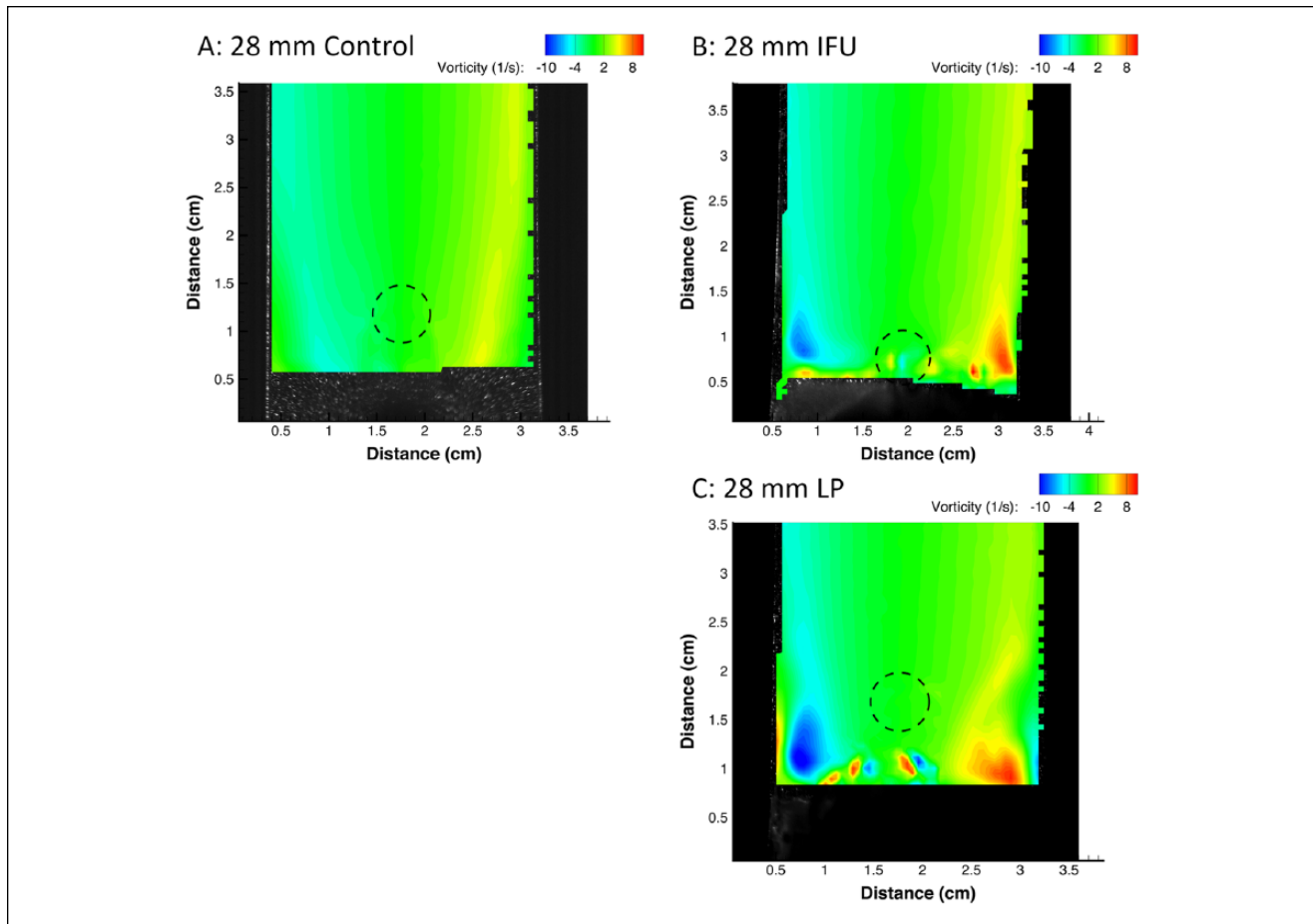


Figure 4. The average vorticity near the anterior and posterior wall in the (left) lateral midplane [IFU vs low positioning (LP) of the stents]; (A) 28-mm control, (B) 28-mm IFU, and (C) 28-mm LP model. The renal orifice is indicated with a black circle. IFU, instructions for use.

RA. The OSI and RRT in the RA were near zero in all models, including the controls.

Discussion

The present study has shown that both the position of the Nellix device in the infrarenal neck and the infrarenal neck diameter affect flow profiles in the aorta proximal to the seal zone and in the RA. Although EVAS had only minimal influence on flow profiles and WSS on the lateral suprarenal aortic wall, vorticity with lower WSS and higher OSI and RRT was observed on the anterior wall proximal to the endbags. The vortices had a steady state in the 32-mm IFU model and 28-mm LP model in contrast to the 24- and 28-mm IFU models where they resolved at the end of a cycle. In the 32-mm IFU model, the enhanced vorticity may have been caused by the larger mismatched area at the transition between the aortic flow lumen and the stents. The observed peak velocity was lower in the 32-mm IFU model compared with the 24-mm and 28-mm IFU models due to

its larger diameter. The lower velocity may have also contributed to prolonged vorticity. Lower positioning of the stent in the 28-mm LP model led to prolonged flow recirculation proximal to the endbags and was potentially associated with the creation of a cul-de-sac volume between the RA and the endbags. The flow is likely to be redirected by the endbags, causing recirculation of flow, potentially leading to the formation of vortices.

The vorticity in the vessels is usually increased near branches and bifurcations where flow separation occurs but usually without steady state.^{19,20} Vortices that were sustained over 1 cardiac cycle (>1 second) were observed only in the 32-mm IFU and 28-mm LP models. Absolute residence times in the order of seconds have been associated with thrombus formation.^{21,22} The RRT does not provide an absolute time for the presence of particles in regions of flow recirculation. The pulsatile inflow signal causes a varying location of the vortices that could prevent tracer particles from residing proximal to the endbags for seconds. It is unknown what the effect of a (stationary) vortex proximal to the endbags will be. Very

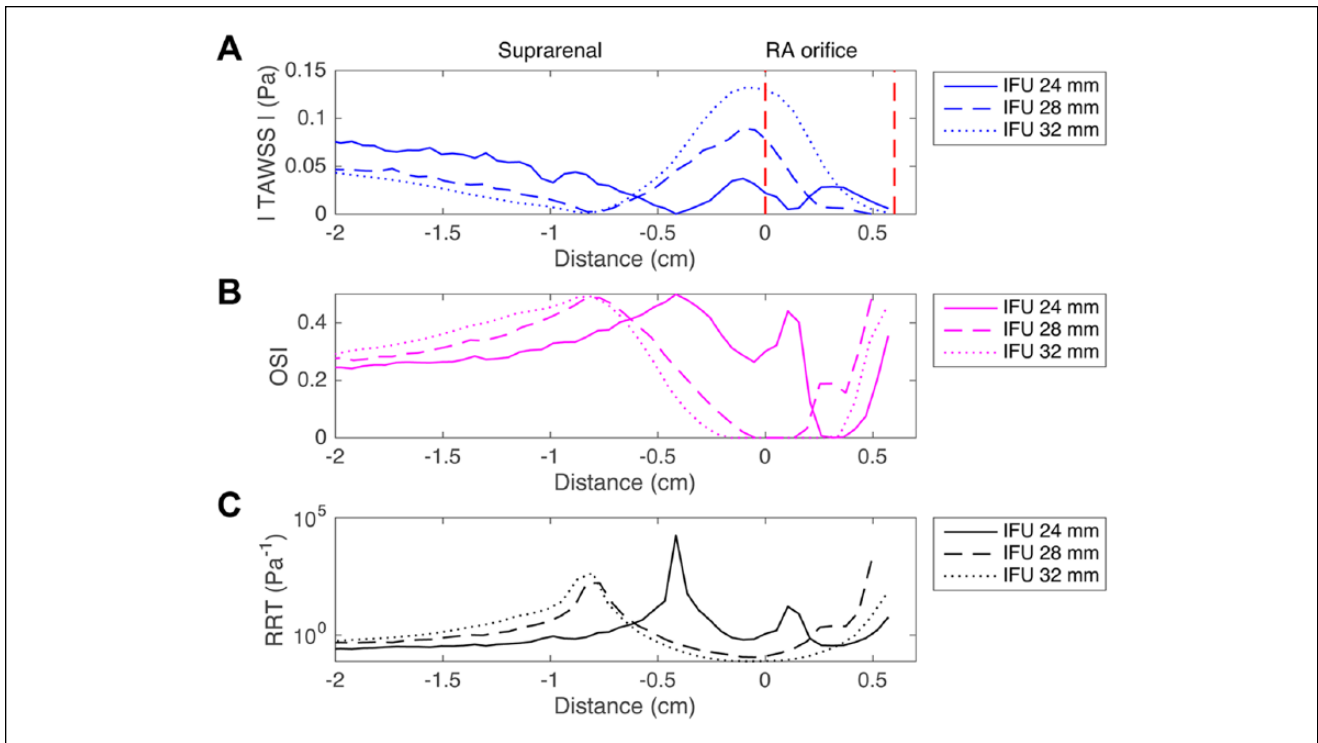


Figure 5. (A) Time-averaged wall shear stress (TAWSS), (B) oscillatory shear index (OSI), and (C) relative residence time (RRT) on the anterior wall of the suprarenal aorta [instructions for use (IFU) comparison]. The renal artery orifice is located between 0 and 0.6 cm.

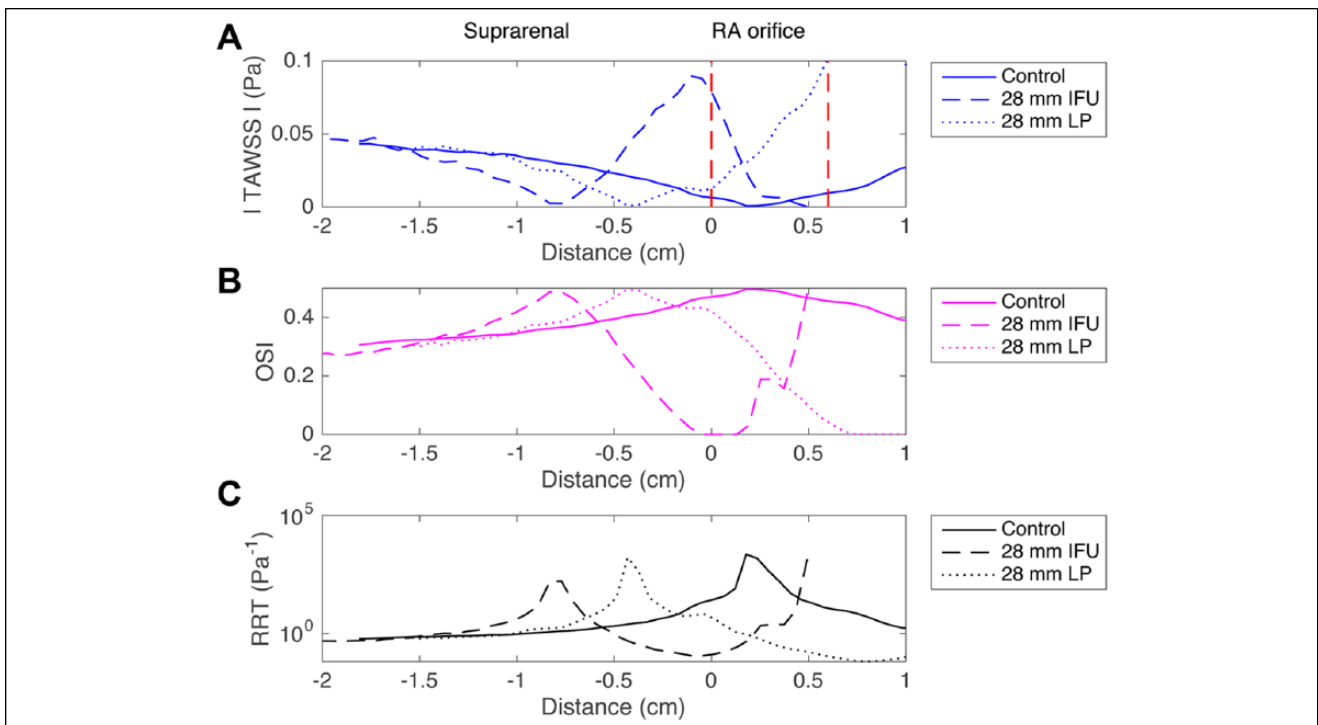


Figure 6. (A) Time-averaged wall shear stress (TAWSS), (B) oscillatory shear index (OSI), and (C) relative residence time (RRT) on the anterior wall of the suprarenal aorta [instructions for use (IFU) vs low positioning (LP) of the endosystem]. The renal artery orifice is located between 0 and 0.6 cm.

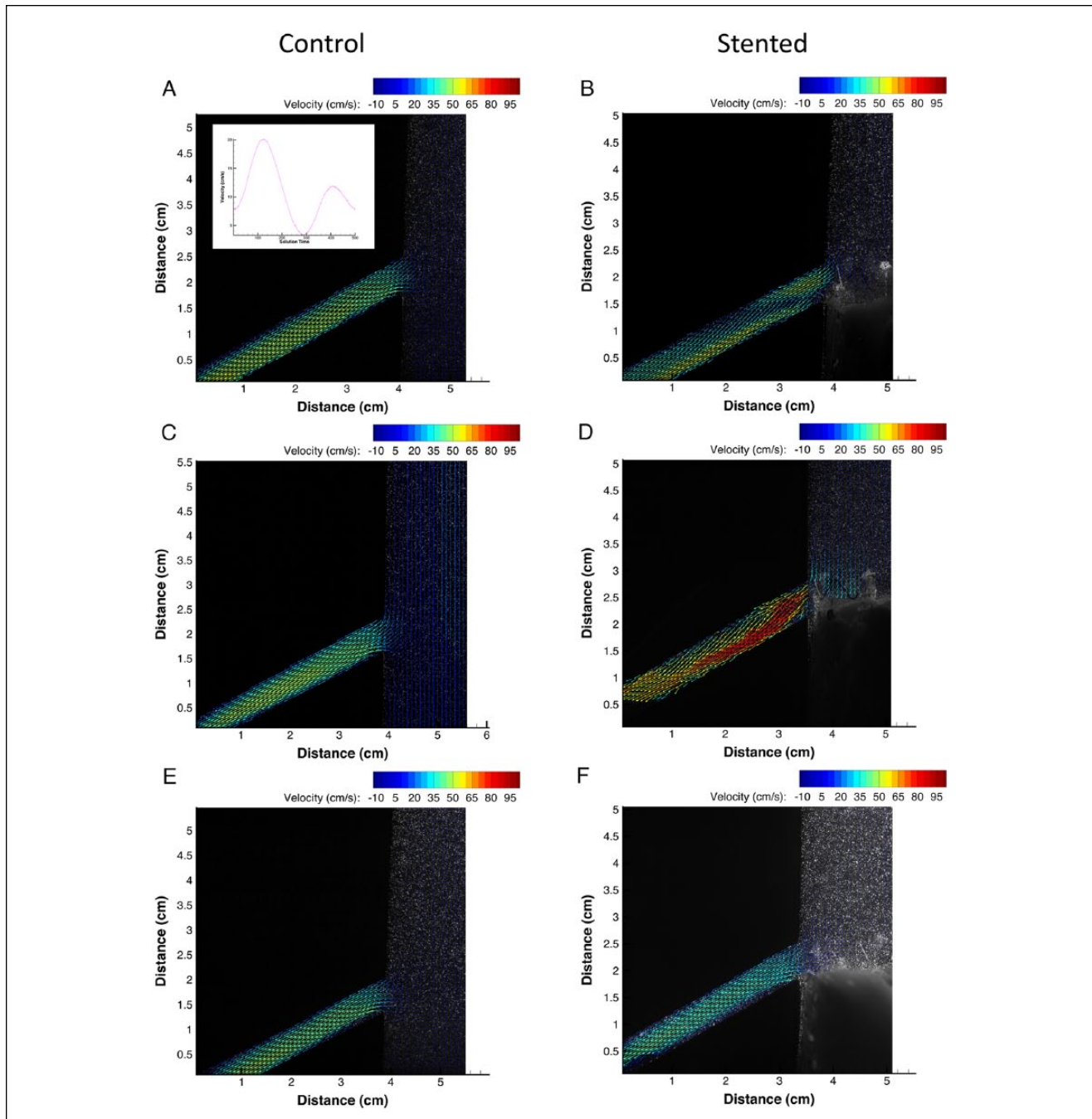


Figure 7. Flow in the renal artery during the peak systolic phase; (A) 24-mm control, (B) 24-mm IFU, (C) 28-mm control, (D) 28-mm IFU, (E) 32-mm model, and (F) 32-mm IFU model. IFU, instructions for use.

few events of thrombus formation have been reported post EVAS. Remodeling of the infrarenal neck with thrombus has been reported in only one case on computed tomography angiography at 30 days after EVAS.⁶ A recent study of 50 patients 1 year after EVAS showed no thrombus formation in this area (unpublished data).

Distal embolization has been reported in very few cases after EVAS.²³ In 2 patients, distal embolization was

associated with anatomical causes, and in 1 patient there was no clear focus. Also, other factors could be involved (ie, arrhythmia). A relation with suboptimal stent expansion or billowing of the covering material that could reduce the flow lumen might have been involved. Remodeling of the infrarenal neck with thrombus may also be protective by neutralizing flow recirculation and preventing embolization.

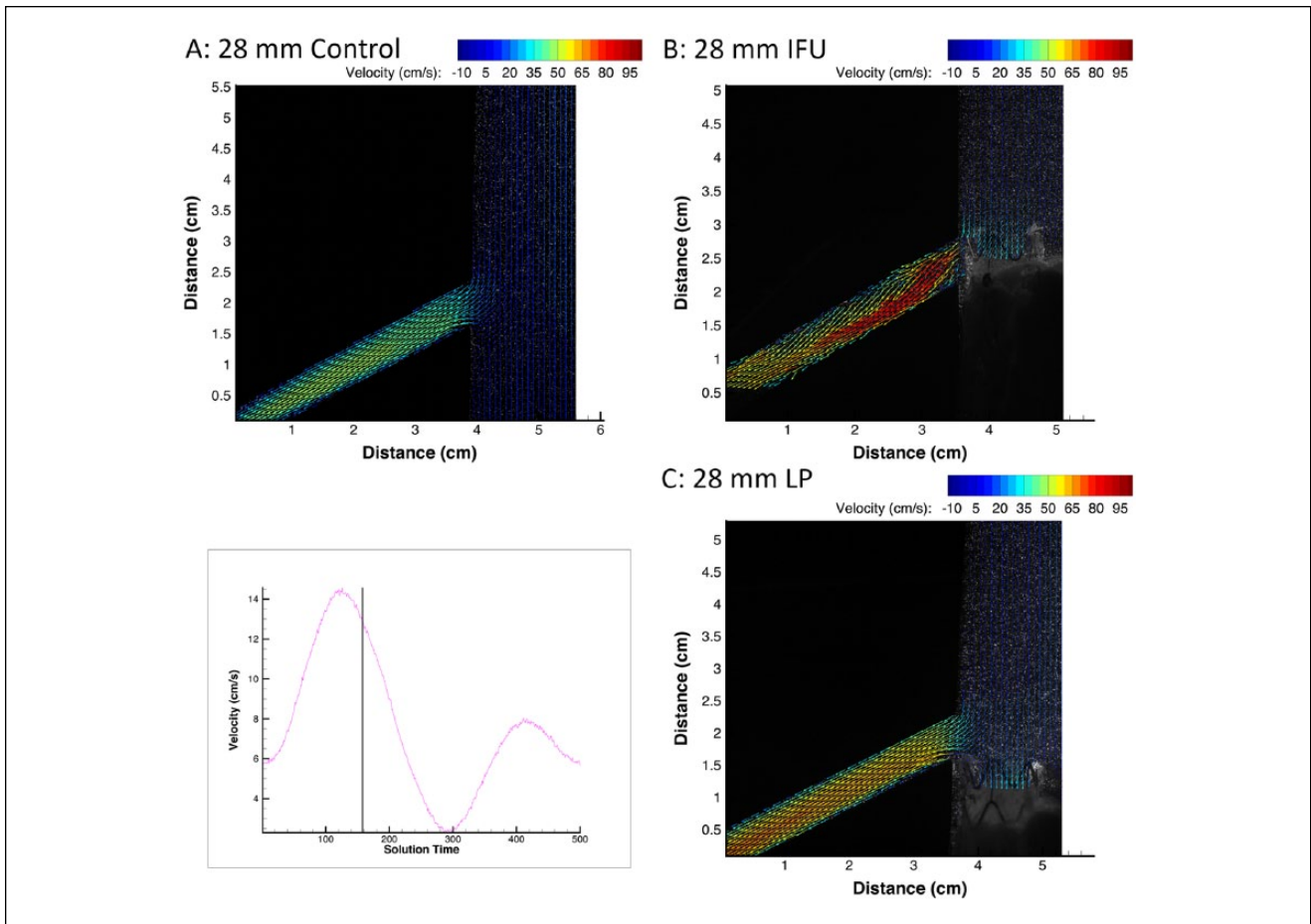


Figure 8. Flow in the renal artery during the peak systolic phase [IFU vs low positioning (LP) of the endosystem]; (A) 28-mm control, (B) 28-mm IFU, (C) 28-mm LP. IFU, instructions for use.

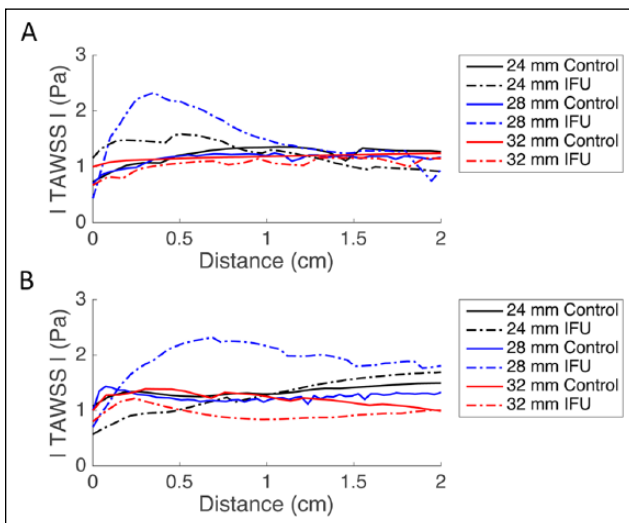


Figure 9. Time-averaged wall shear stress (TAWSS) of the renal artery plotted vs the longitudinal distance along the vessel wall (IFU comparison); (A) cranial wall, (B) caudal wall. The renal artery orifice is located at a distance of 0 cm. IFU, instructions for use.

Lower values for baseline WSS have been reported for the abdominal aorta in a range of -0.17 to 0.14 Pa.¹¹ The locations with the lowest WSS were found near the aortic bifurcation and correlated well (near zero) with the locations with enhanced atherosclerosis measured by intimal thickness. In the present study, the regions that presented a very low TAWSS ($<10^{-2}$ Pa) were small in both controls and stented models. Additionally, both controls and stented models showed a peak OSI of 0.5 and increase in the RRT in some areas in the suprarenal aorta, although the location was more cranial in the suprarenal aorta in the stented models compared to the controls. Small regions of low WSS and high OSI (0.5) were found in areas on the infrarenal aortic wall (ie, juxtarenal) of healthy subjects, and it is unknown whether these will enhance atherosclerosis.²⁴ A recent review by Peiffer et al²⁵ demonstrated that a discrepancy persists regarding the role of low shear and high OSI in the development of atherosclerosis. The effects of low WSS and high OSI after EVAS are unknown. The area of lower WSS in the RA in the 24- and 28-mm IFU models (<1 Pa) was small

(<2 mm), but still atherosclerosis may be enhanced or vascular remodeling may occur in this region.

The stronger jet flow and higher velocity in the RA in the 24- and 28-mm IFU models may be caused by excessive endobag material in the neck or by partial coverage of the RA orifice due to proximal stent positioning. Positioning variability of the stents in EVAS may be caused by minor changes in stent position during injection of the polymer, as the stents should be held in position by one of the operators. In vivo, aortic movement may also be involved.

The 28-mm IFU model showed the largest increase in peak velocity (around 70%) compared with the control. This phenomenon was also observed in a previous flow study on EVAS with the 28-mm IFU model,²⁶ showing that maximum shear rate associated with this increase in peak velocity in the RA is well below the pathological threshold for acute thrombosis, so this event should not be expected.²⁶ The computational fluid dynamics study conducted by Segalova and coauthors²⁷ has demonstrated that the proximal bare stent had almost no influence on the renal flow profile when positioned across the RA orifice, and it is not likely that the proximal bare metal stent will cause large disturbances in RA flow profile. An intended positioning with the bare metal stent across the RA ostium (proximal 4 mm) should be a safe margin for positioning of the endosystem with reference to the RA orifice. This positioning will lead to an optimal use of the available infrarenal neck and maximize the seal zone in this area.

The present study showed that the endobags had a different morphology in all models and a different location of the proximal stents in the aorta in all configurations (Figure 1A-D). It therefore seems that there is also variability in positioning of the endosystem, especially when considering the large variance in human anatomy. Future developments should focus on reducing variability of the proximal expansion of the endobag and avoiding excessive endobag material in the infrarenal neck. In EVAR, the proximal sealing zone is clearly marked by radiopaque markers on the stent fabric or frame, and this is supposed to enable a more predictable positioning of the proximal stents with reference to the most caudal RA.

Limitations

A drawback of a 2-element windkessel model is that pressure and flow are out of phase. A 3-element windkessel model may also be applied; however, this mainly benefits the relation between blood pressure and blood flow. This is important, but of less interest in the present study, where the focus was on flow dynamics.

A straightforward anatomy was used to study positioning of the EVAS endosystem on flow in the suprarenal aorta and RA. A different geometry, that is, inclusion of aortoiliac angulations, asymmetric location of RA orifices, and

inclusion of other branches (superior mesenteric artery) could have led to other flow profiles. Thus, the results of this study cannot be generalized for all patients who undergo EVAS. Moreover, the flow was examined at physiological resting conditions (60 beats per minute), whereas other in vitro studies have shown that flow changes can be expected at a higher heart rate.¹² It is presently unknown how a higher heart rate (and blood pressure) will affect flow post EVAS.

Furthermore, the flow rate was similar in all flow tests, which clinically might not be the case. A patient with a larger aortic diameter might have a larger cardiac output compared with a patient with a smaller aortic diameter. The abdominal aortic flow rate of 1.6 L/min at rest was used in a previous in vitro study.¹⁴ This flow rate was close to the lower boundary of physiological flow at rest, corresponding to a cardiac output of 4 L/min. A lower flow rate was selected as the cardiac output usually decreases in the elderly.

This study demonstrated that stationary vortices occur proximal to the endobags in a 32-mm aorta at low flow rates. It is supposed that a larger flow rate in a 32-mm aorta will lead to an even higher degree of flow recirculation, as the Reynolds number increases. It is unknown how long individual particles will reside proximal to the endobags in the 32-mm IFU and 28-mm LP models. Particle tracking velocimetry may allow tracking of individual particles and calculation of absolute residence times and may provide a better understanding of the risk for thrombus formation proximal to the endobags. A dye injection to visualize (individual) fluid streams could be an alternative approach to study the (absolute) particle residence time.²⁸ Recent updates to the Nellix IFU were made, excluding treatment of AAA with an infrarenal neck diameter >28 mm.

Blood has been demonstrated as Newtonian for flow in large vessels, but it has a shear-thinning behavior for flow in small vessels (<6 mm). WSS in the RA may therefore be slightly overestimated in comparison to the in vivo situation. In addition, a no-slip boundary condition was used with zero velocity at the vessel wall for the calculation of the shear rate, which may have added to a steeper velocity gradient near the wall, resulting in an overestimation of WSS. The assumption of using a rigid model during the flow tests may be justified by stiffening of the vasculature in atherosclerotic disease.

Conclusion

The EVAS endosystem enhances vorticity in the suprarenal aorta, mostly in larger diameter necks and when the stents are positioned low. A positioning of the endobags just below the RA affects the flow profile in a small area of the RA in 24- and 28-mm diameter necks, while a low positioning of the stents does not influence the RA flow profile.

Declaration of Conflicting Interests

The author(s) declared the following potential conflicts of interest with respect to the research, authorship, and/or publication of this article: Jean-Paul P. M. de Vries and Michel M. P. J. Reijnen are consultants for Endologix Inc.

Funding

The author(s) disclosed receipt of the following financial support for the research, authorship, and/or publication of this article: The stents and materials for this study were sponsored by Endologix Inc.

Supplemental Material

The online videos are available at <http://journals.sagepub.com/doi/suppl/10.1177/1526602817719465>

References

1. Thompson MM, Heyligers JM, Hayes PD, et al, for the EVAS FORWARD Global Registry Investigators. Endovascular aneurysm sealing: early and midterm results from the EVAS FORWARD Global Registry. *J Endovasc Ther.* 2016;23:685–692.
2. van den Ham LH, Zeebregts CJ, de Vries JP, et al. Abdominal aortic aneurysm repair using Nellix endovascular aneurysm sealing. *Surg Technol Int.* 2015;26:226–231.
3. Moll F, Powell J, Fraedrich G, et al; European Society for Vascular Surgery. Management of abdominal aortic aneurysms clinical practice guidelines of the European Society for Vascular Surgery. *Eur J Vasc Endovasc Surg.* 2011;41(suppl 1):S1–S58.
4. Carpenter JP, Cuff R, Buckley C, et al; Nellix Investigators. One-year pivotal trial outcomes of the Nellix system for endovascular aneurysm sealing. *J Vasc Surg.* 2017;65:330–336.e4.
5. Youssef M, Nurzai Z, Zerwes S, et al. Initial experience in the treatment of extensive iliac artery aneurysms with the Nellix Aneurysm Sealing System. *J Endovasc Ther.* 2016;23:290–296.
6. Holden A, Savlovskis J, Winterbottom A, et al. Imaging after Nellix endovascular aneurysm sealing: a consensus document. *J Endovasc Ther.* 2016;23:7–20.
7. Lowe GD. Virchow's triad revisited: Abnormal flow. *Pathophysiol Haemost Thromb.* 2003;33:455–457.
8. Hathcock JJ. Flow effects on coagulation and thrombosis. *Arterioscler Thromb Vasc Biol.* 2006;26:1729–1737.
9. Malek AM, Alper SL, Izumo S. Hemodynamic shear stress and its role in atherosclerosis. *JAMA.* 1999;282:2035–2042.
10. Ku DN, Giddens DP, Zarins CK, et al. Pulsatile flow and atherosclerosis in the human carotid bifurcation. positive correlation between plaque location and low oscillating shear stress. *Arteriosclerosis.* 1985;5:293–302.
11. Moore JE, Xu C, Glagov S, et al. Fluid wall shear stress measurements in a model of the human abdominal aorta: oscillatory behavior and relationship to atherosclerosis. *Atherosclerosis.* 1994;110:225–240.
12. Pedersen EM, Agerbaek M, Kristensen IB, et al. Wall shear stress and early atherosclerotic lesions in the abdominal aorta in young adults. *Eur J Vasc Endovasc Surg.* 1997;13:443–451.
13. Groot Jebbink E, Mathai V, Boersen JT, et al. Hemodynamic comparison of stent configurations used for aortoiliac occlusive disease. *J Vasc Surg.* 2017;66:251–260.e1.
14. Moore JE, Ku DN. Pulsatile velocity measurements in a model of the human abdominal aorta under resting conditions. *J Biomech Eng.* 1994;116:337–346.
15. Yousif MY, Holdsworth DW, Poepping TL. A blood-mimicking fluid for particle image velocimetry with silicone vascular models. *Exp Fluids.* 2011;50:769–774.
16. Thielicke W, Stamhuis EJ. PIVlab—towards user-friendly, affordable and accurate digital particle image velocimetry in MATLAB. *J Open Res Softw.* 2014;2:e30.
17. He X, Ku DN. Pulsatile flow in the human left coronary artery bifurcation: average conditions. *J Biomech Eng.* 1996;118:74–82.
18. Himburg HA, Grzybowski DM, Hazel AL, et al. Spatial comparison between wall shear stress measures and porcine arterial endothelial permeability. *Am J Physiol Heart Circ Physiol.* 2004;286:H1916–H1922.
19. Zarins CK, Giddens DP, Bharadvaj BK, et al. Carotid bifurcation atherosclerosis. quantitative correlation of plaque localization with flow velocity profiles and wall shear stress. *Circ Res.* 1983;53:502–514.
20. van der Laan PA, Reardon CA, Getz GS. Site specificity of atherosclerosis: site-selective responses to atherosclerotic modulators. *Arterioscler Thromb Vasc Biol.* 2004;24:12–22.
21. Reininger AJ, Reininger CB, Heinzmann U, et al. Residence time in niches of stagnant flow determines fibrin clot formation in an arterial branching model—detailed flow analysis and experimental results. *Thromb Haemost.* 1995;74:916–922.
22. Basciano C, Kleinstreuer C, Hyun S, et al. A relation between near-wall particle-hemodynamics and onset of thrombus formation in abdominal aortic aneurysms. *Ann Biomed Eng.* 2011;39:2010–2026.
23. Zerwes S, Nurzai Z, Leissner G, et al. Early experience with the new endovascular aneurysm sealing system Nellix: first clinical results after 50 implantations. *Vascular.* 2016;24:339–347.
24. Sugimoto K, Shimamura Y, Tezuka C, et al. Effects of arterial blood flow on walls of the abdominal aorta: distributions of wall shear stress and oscillatory shear index determined by phase-contrast magnetic resonance imaging. *Heart Vessels.* 2016;31:1168–1175.
25. Peiffer V, Sherwin SJ, Weinberg PD. Does low and oscillatory wall shear stress correlate spatially with early atherosclerosis? A systematic review. *Cardiovasc Res.* 2013;99:242–250.
26. Boersen JT, Groot Jebbink E, Versluis M, et al. Flow and wall shear stress characterization following endovascular aneurysm repair and endovascular aneurysm sealing in an infrarenal aneurysm model [published online March 9, 2017]. *J Vasc Surg.* doi:10.1016/j.jvs.2016.10.077.
27. Segalova PA, Rao KV, Zarins CK, et al. Computational modeling of shear-based hemolysis caused by renal obstruction. *J Biomech Eng.* 2012;134:021003.
28. Groot Jebbink E, Goverde P, van Oostayen J, et al. Innovation in aortoiliac stenting: an in vitro comparison. Proc SPIE 9036, Medical Imaging 2014: Image-Guided Procedures, Robotic Interventions, and Modeling, 90361X (March 12, 2014).